Specific Activation of the CD271 Intracellular Domain in Combination with Chemotherapy or Targeted Therapy Inhibits Melanoma Progression

Annalisa Saltari[1], Andreas Dzung[1], Marika Quadri[2], Natascia Tiso[3], Nicola Facchinello[3], Alberto Hernández-Barranco[4], Susana Garcia-Silva[4], Laura Nogués[4], Corinne Isabelle Stoffel[1], Phil F. Cheng[1], Patrick Turko[1], Ossia M. Eichhoff[1], Francesca Truzzi[2,5], Alessandra Marconi[2], Carlo Pincelli[2], Héctor Peinado[4], Reinhard Dummer[1], and Mitchell P. Levesque[1]

ABSTRACT

CD271 (NGFR) is a neurotrophin receptor that belongs to the tumor necrosis receptor (TNFR) family. Upon ligand binding, CD271 can mediate either survival or cell death. Although the role of CD271 as a marker of tumor-initiating cells is still a matter of debate, its role in melanoma progression has been well documented. Moreover, CD271 has been shown to be upregulated after exposure to both chemotherapy and targeted therapy. In this study, we demonstrate that activation of CD271 by a short β-amyloid–derived peptide ($A\beta^{(25-35)}$) in combination with either chemotherapy or MAPK inhibitors induces apoptosis in 2D and 3D cultures of eight melanoma cell lines. This combinatorial treatment significantly reduced metastasis in a zebrafish xenograft model and led to significantly decreased tumor volume in mice. Administration of $A\beta^{(25-35)}$ in *ex vivo* tumors from immunotherapy- and targeted therapy–resistant patients significantly reduced proliferation of melanoma cells, showing that activation of CD271 can overcome drug resistance. $A\beta^{(25-35)}$ was specific to CD271-expressing cells and induced CD271 cleavage and phosphorylation of JNK (pJNK). The direct protein–protein interaction of pJNK with CD271 led to PARP1 cleavage, p53 and caspase activation, and pJNK-dependent cell death. $A\beta^{(25-35)}$ also mediated mitochondrial reactive oxygen species (mROS) accumulation, which induced CD271 overexpression. Finally, CD271 upregulation inhibited mROS production, revealing the presence of a negative feedback loop in mROS regulation. These results indicate that targeting CD271 can activate cell death pathways to inhibit melanoma progression and potentially overcome resistance to targeted therapy.

Significance: The discovery of a means to specifically activate the CD271 death domain reveals unknown pathways mediated by the receptor and highlights new treatment possibilities for melanoma.

Introduction

CD271 (p75NTR, NGFR) is a transmembrane receptor expressed in the nervous system and skin. It interacts with numerous ligands to modulate multiple pathways (1–6). The known ligands are the four neurotrophins. CD271 can bind the neurotrophins alone or in association with another class of neurotrophin receptors: the tropomyosin receptor kinases (TrkA, TrkB, and TrkC). Interestingly, melanoma cells synthesize and secrete all neurotrophins and express both receptor classes, revealing the presence of a complex autocrine pathway regulating proliferation and migration (7).

Several studies showed that CD271 plays a critical function in melanoma (6–10). CD271 downregulation increases cell proliferation, whereas its overexpression is associated with a stem-like quiescent state. In contrast, its role in metastasis remains controversial. CD271 expression was shown to be lost in early progression when melanoma cells invade the dermis (11), whereas other studies showed its association with increased metastatic abilities (8, 10).

Live-cell imaging revealed that exposure of melanoma cells to MAP-kinase inhibitors (MAPKi) results in multiple cell fates including a drug-adapted state associated with CD271 overexpression, reversible upon drug removal (5). Consistently, Rambow and colleagues identified drug-tolerant transcriptional states in BRAF-mutant patient-derived xenografts exposed to MAPKi, showing CD271 to be one of the key markers of adaptive resistance (12).

CD271 expression is upregulated in response to chemotherapeutic agents in association with DNA repair genes, revealing a role in chemoresistance (13, 14). Notably, some studies demonstrated CD271 to be a suppressor of p53 leading to MDM2-mediated p53 proteolysis (15).

CD271 can signal alone or in association with other receptors (e.g., Trks, Nogo, sortilin, DR6), promoting either survival or apoptosis. This flexibility allows CD271 to play a fundamental role in the regulation of cell fate by acting as an on/off switch to modulate opposing pathways (6).

Unlike neurotrophins, which bind CD271 and activate opposite pathways according to the cell tissue context, β-amyloid has been shown to bind CD271 with a high affinity and to selectively activate its apoptotic pathway in the nervous system (16).

[1]Department of Dermatology, University of Zurich Hospital, University of Zurich, Zurich, Switzerland. [2]Laboratory of Cutaneous Biology, Department of Surgical, Medical, Dental and Morphological Sciences, University of Modena and Reggio Emilia, Modena, Italy. [3]Laboratory of Developmental Genetics, Department of Biology University of Padova, Padova, Italy. [4]Microenvironment and Metastasis Laboratory, Molecular Oncology Programme, Spanish National Cancer Research Center (CNIO), Madrid, Spain. [5]Department of Agricultural and Food Science, University of Bologna, Bologna, Italy.

Corresponding Author: Mitchell P. Levesque, Department of Dermatology, University Hospital of Zurich, Wagistrasse 18, Zurich 8952, Switzerland. E-mail: mitchell.levesque@usz.ch

Cancer Res 2021;81:6044–57

doi: 10.1158/0008-5472.CAN-21-0117

Unlike previous approaches that inhibited the receptor or prevented its overexpression, we activated the CD271 pro-apoptotic function with a short β-amyloid derived peptide. Since the minimum sequence able to bind CD271 was shown to be amino acids 25–35, all experiments were performed using this short peptide ($A\beta^{(25-35)}$; refs. 17–20).

Materials and Methods

Cell culture

WM115, WM266–4, SKMEL28, WM793B, and 1205Lu (ATCC) were cultured as indicated by the manufacturer. Other cell lines were generated from biopsies at the University Hospital Zurich after written informed consent and approval by the local Institutional Review Board (BASEC-2017–0494) as previously described (21). The cultures p0-p20 were tested for *Mycoplasm* once a month. Cells were grown in RPMI1640 (Sigma Life Science) supplemented with 10% FBS (Gibco, Life Technologies), 2 mmol/L glutamine (Biochrom), and sodium-pyruvate (Sigma Life Science). Human cells experiments were approved by the ethical review board (KEK No. 2014–0425).

Drugs used: PLX4032 and MEk162 (Selleckchem), JNKi (SP600125, Santa Cruz Biotechnology), MG132, DAPT and TAPI2 (Calbiochem), N-acetyl-L-cysteine (Sigma), cisplatin, dacarbazine, and carmustine (Selleckchem).

$A\beta^{(25-35)}$ (Bachem; catalog no. H-1192). "Cntr" refers to the inverted sequence$^{(35-25)}$ (Bachem; catalog no. H-2964). Both peptides were diluted in PBS and incubated at 37°C for 2 hours. Fibril formation was induced by sonication (5 seconds, low intensity). For the treatment with soluble ECD, we used the recombinant protein from LSBio (catalog no. LS-G27179).

Ex vivo cultures

Tumor slices were kept in medium with antibiotic and then embedded in 1% agarose on the same day as biopsy. The tumors were cut with a vibratome (300 μm), and the slices were placed on filters in 6-well plates and treated for 3 to 5 days.

Three-dimensional spheroids

A total of 5×10^3 melanoma cells/well were seeded on agarose-coated plates as described previously (22). Seventy-two hours later, melanoma spheroids were implanted into collagen I as described previously (23). For live/dead evaluation, spheres were stained with calcein 7 μmol/L (Sigma, catalog no. 17783) and ethidium homodimer 10 μmol/L (Sigma, catalog no. E1510) for 1 hour in melanoma medium. Pictures were taken with a confocal microscope (Leica TCS SPE). Analysis of spheroids area was performed as described previously (11). Live/dead staining was quantified with Photoshop.

MTT assay

A total of 5×10^3 cells/well were seeded in 96-well plates. Cells were incubated with 0.5% MTT for 4 hours at 37°C and then dissolved with 100 μL isopropanol. The plate was read at 560 nm with a reference filter of 650 nm.

Flow cytometry

Cells were incubated with anti-CD271 antibody (1:100 in PBS; Merck, catalog no. 05–446) and with secondary Alexa Fluor anti-mouse 488 (1:50; Invitrogen, catalog no. A21202) for 20 minutes at 4°C and analyzed by flow cytometry (LSR Fortessa II).

Reactive oxygen species (ROS) measurements: cells were stained with MitoSOX (5 μM; Invitrogen, catalog no. M36008) for 20 minutes at room temperature, resuspended in FACS Buffer (0.2% FBS in PBS) and analyzed. For cell death analysis, cells were stained with PI solution (50 μg/mL propidium iodide, 0.1% sodium citrate, 0.5% Tryton X-100) for 15 minutes. For caspase-3 staining, the "CellEvent Caspase-3/7 green detection Reagent" Kit (Invitrogen, C10723) was used.

Cell sorting

Cells were incubated in blocking buffer (DMEM, 10% FBS, 4% human gamma globulin) for 20 minutes on ice. Cells were stained with anti-CD271 antibody (1:100 in PBS, Merck, catalog no. 05–446) at room temperature for 15 minutes, washed and stained with Alexa Fluor 488 anti-mouse antibody (Invitrogen, catalog no. A21202) for 15 minutes at room temperature. Melanoma medium was added to the cells. A FACS Aria III flow cytometer (BD Biosciences) was used and analyzed on FACS Diva software (BD Biosciences).

Skin reconstructs

Reconstructs were generated by seeding human keratinocytes and melanoma cells on dermal equivalents, as described previously (11). After 12 days, skin reconstructs were fixed with formalin for 2 hours at room temperature and embedded in paraffin.

Western blotting

Cells were harvested in lysis buffer pH 7.5 (150 mmol/L NaCl, 15 mmol/L MgCl, 1 mmol/L EGTA, 50 mmol/L Hepes, 10% Glicerol, 1% Triton-X100). Membranes were incubated with CD271 (1:1000, Cell Signaling Technology, catalog no. 8238), CD271_ICD (1:1000; Merck, catalog no. 07–476), APR1 (1:1,000; Thermo Fisher Scientific, catalog no. PA5–67686), NRAGE (1:250; R&D System, catalog no. MAB38352), PARP (1:1,000; Cell Signaling Technology, catalog no. 9542), cleaved-PARP (1:1,000; Cell Signaling Technology, catalog no. 5625), p53 (1:1,000; Cell Signaling Technology, catalog no. 2527), p21 (1:500; Cell Signaling Technology, catalog no. 2946), GSK (1:1,000; Cell Signaling Technology, catalog no. 9315), pGSK (1:1,000; Cell Signaling Technology, catalog no. 9336), JNK (1:1000; Cell Signaling Technology, catalog no. 9252), pJNK (1:1,000; Cell Signaling Technology, catalog no. 4668), GAPDH (1:500; Cell Signaling Technology, catalog no. 3683), Snail (1:1,000; Cell Signaling Technology, catalog no. 3879), Slug (1:1,000; Cell Signaling Technology, catalog no. 9585), N-cadherin (1:1,000; Cell Signaling Technology, catalog no. 13116), E-cadherin (1:1,000; Cell Signaling Technology, catalog no. 3195), and secondary peroxidase-conjugated antibody (1:3,000; Cell Signaling Technology, catalog no. 7074).

Protein immunoprecipitation

The immunoprecipitation kit (Abcam; catalog no. ab206996) was used in pull down experiments. M121224 wt and CD271 KO cells were treated for 48 hours with $A\beta^{(25-35)}$ 40 μmol/L. Lysates were pulled-down with CD271 Ab (1 μg Ab/300 μg lysate).

Melanoma cell infection

Lentiviral vectors [CD271 full-length and extracellular domain (ECD) overexpression] were a gift from Lukas Sommer (8). For CD271 transient induction, M130429 melanoma cells with inducible CMVTO_EV and CMVTO_CD271 constructs, were induced *in vitro* with doxycycline at a concentration of 1 μg/mL as described previously (8).

CRISPR/cas9 KO

CD271-specific sgRNAs (GGTGTCCCTTGGAGGTGCCA) were used. HEK293T, cells were seeded for transfection with the viral

plasmids. After 24 hours, the LentiCRISPRv2GFP expression plasmid (Addgene, plasmid no. 82242426, catalog no. 82416) containing CD271 sgRNA was mixed with the packaging plasmid psPAX2 (2 μg; Addgene, plasmid no. 12260), the envelope plasmid pMD2.G (1 μg; Addgene, plasmid no. 12259), and PEImax (21 μg; Polysciences, catalog no. 24765) in 1 mL of serum-free DMEM (Gibco, catalog no. 11960–044) and incubated 15 minutes at room temperature. The DNA/PEImax mixture was add to the HEK293T cells and the medium was collected and sterile filtered 48 hours. Melanoma cells were incubated overnight in virus-containing medium + 8 μg/mL polybrene (H9268, Sigma-Aldrich). GFP-positive cells were sorted by the FACSAria III (BD Biosciences).

Cell transfection with siRNA

Cells plated for 24 hours in antibiotic-free medium were transfected with 100 nmol/L APR1 (OnTargetPlus SMART pool human MAGEH1, catalog no. L-009135-00-0005) or scrambled siRNA (Dharmacon Inc.; Scramble, siGENOME Control pool Non-targeting #1, catalog no. D-001206-13-05) in antibiotic/FBS-free medium for 24, 48, and 72 hours. For transfection we used the INTERFERin Transfection Kit (Polyplus-transfection, catalog no. 101000016) and we followed the manufacturer's guidelines.

IHC

Skin reconstructs and melanoma lesions were stained with hematoxylin and eosin (H&E), S100 (1:400; Novocastra, Agilent Technologies, catalog no. NCL-L-S100p), CD271 (1:100 in PBS; Lab Vision Corporation, catalog no. LS-C124234-100), Ki67 (1:200 in PBS; Dako, catalog no. M7240), TUNEL (Sophistolab), Snail/Slug (1:500 in PBS, Abcam, ab85936) and caspase-3 (1:800, Abcam ab2302).

Zebrafish

Zebrafish experiments were performed at the University of Padova, Italy, under authorization 407/2015-PR (OPBA). All procedures complied with the European Legislation for the Protection of Animals used for Scientific Purposes (Directive 2010/63/EU). Embryos were obtained from natural spawning of albino adults. Human cells were stained with Vybrant Cell-Labeling Solution (5 μg/mL, Molecular Probes) for 20 minutes, loaded in a glass capillary needle, and microinjected into the yolk as previously described (11). Analysis was performed by a blind investigator. Imaging was performed using a Leica MZFLIII dissecting microscope with a Leica DFC7000T camera.

Mice

For *in vivo* experiments 9-week-old female Hsd:Athymic Nude-Foxn1nu were used.

All animals were housed according to institutional guidelines and experiments were approved by CNIO, the ISCIII Ethical Committee, and the Comunidad Autónoma de Madrid (protocol PROEX225/17). The experiments were performed in accordance to the guidelines for Ethical Conduct in the Care and Use of Animals as stated in The International Guiding Principles for Biomedical Research involving Animals, developed by the Council for International Organizations of Medical Sciences (CIOMS). 5×10^5 M121224 cells were subcutaneously injected in 40 μL of 1:1 DMEM: Matrigel (BD Biosciences) and when the tumor reached 50 mm^3, 15 μg of $A\beta^{(25-35)}$/BSA in 20 μL were intratumoral injected three times a week. Mice were sacrificed when control group reached 1,000 mm^3.

Statistical analysis

Statistical analysis was performed using GraphPad Prism5.0. *P* values ≤0.05 were considered significant. Cell line experiments were triplicated and error bars represent the mean ± SD. Student *t* test or 2-way ANOVA were applied.

Data availability

The authors declare that the data of this study are available within the paper and its supplementary files or from the authors upon request.

Results

CD271 is upregulated by chemo- or MAPKi therapy

CD271 marks neural crest-like cells that are associated with resistance to targeted therapy (12). We thus evaluated its expression after treatment with carmustine (BCNU), cisplatin (CISP), and dacarbazine (DTIC) in ATCC cell lines (**Fig. 1A**). All chemotherapies strongly induced CD271 expression. In WM115 cells, CD271 dramatically increased from 32.51% to 85.51% (BCNU), 94.59% (CISP), and 95.22% (DTIC); in WM266–4 cells from 27.53% to 66.76% (BCNU), 56.06% (CISP), and 89.37% (DTIC) and in SKMEL28 cells, from 2.11% to 25.86% (BCNU), 85.50% (CISP), and 54.59% (DTIC).

We next assessed the response to MAPK inhibitors in cells extracted from eight melanoma patients' metastases. At a basal level, CD271 was heterogeneously expressed (Supplementary Fig. S1A). Confirming previous results, cisplatin induced a strong upregulation of CD271 in all cells, independent of the driver mutation (**Fig. 1B**; Supplementary Fig. S1B). A strong increase was also observed following treatment with vemurafenib (PLX4032, BRAFi), binimetinib (MEK162, MEKi), alone or in combination (**Fig. 1B**; Supplementary Fig. S1B). We confirmed this on matched tumor biopsies collected before and after the patients received BRAFi+MEKi therapy. We observed that CD271 was significantly higher after targeted therapy ($P < 0.01$; **Fig. 1C** and **D**; Supplementary Fig. S1C).

To study the role of CD271 in drug resistance, we evaluated its expression in three-dimensional (3D) spheroids derived from resistant and sensitive melanoma cells. Interestingly, MAPKi-resistant spheres displayed significantly higher CD271 levels in comparison to sensitive spheres (**Fig. 1E**).

This result was confirmed by comparing CD271 expression in sensitive and resistant subpopulations derived from the same cells after making them resistant *in vitro* through the long-term administration of BRAFi/MEKi (**Fig. 1F**), suggesting that CD271 is associated with acquired resistance. We then induced the stable overexpression of CD271 full length (FL) in 1205Lu cells and we treated the cells. Although no difference was observed with BRAFi, CD271_FL cells showed a significantly reduced sensitivity to MEKi compared with the empty vector (EV; Supplementary Fig. S1D). To better understand the role of CD271 in drug response, we analyzed the correlation between IC_{50} to BRAFi/MEKi and CD271 levels (Supplementary Fig. S1E). However, no significant correlation was observed. We finally checked the expression of multidrug resistant (MDR) proteins, the so called "ATP-binding cassette" (ABC) proteins, which export drugs out of the cell (Supplementary Fig. S1F). None of these showed a correlation with CD271 suggesting resistance mechanisms independent of MDR proteins.

$A\beta^{(25-35)}$ treatment reduces proliferation and induces cell death in 2D and 3D

Given the rapid upregulation of CD271 in response to therapy, we aimed to activate apoptosis in CD271-expressing cells with a short peptide derived from the β-amyloid (Aβ) sequence. All experiments used the short peptide $A\beta^{(25-35)}$ derived from the total $A\beta$ $sequence^{(1-42\ aa)}$.

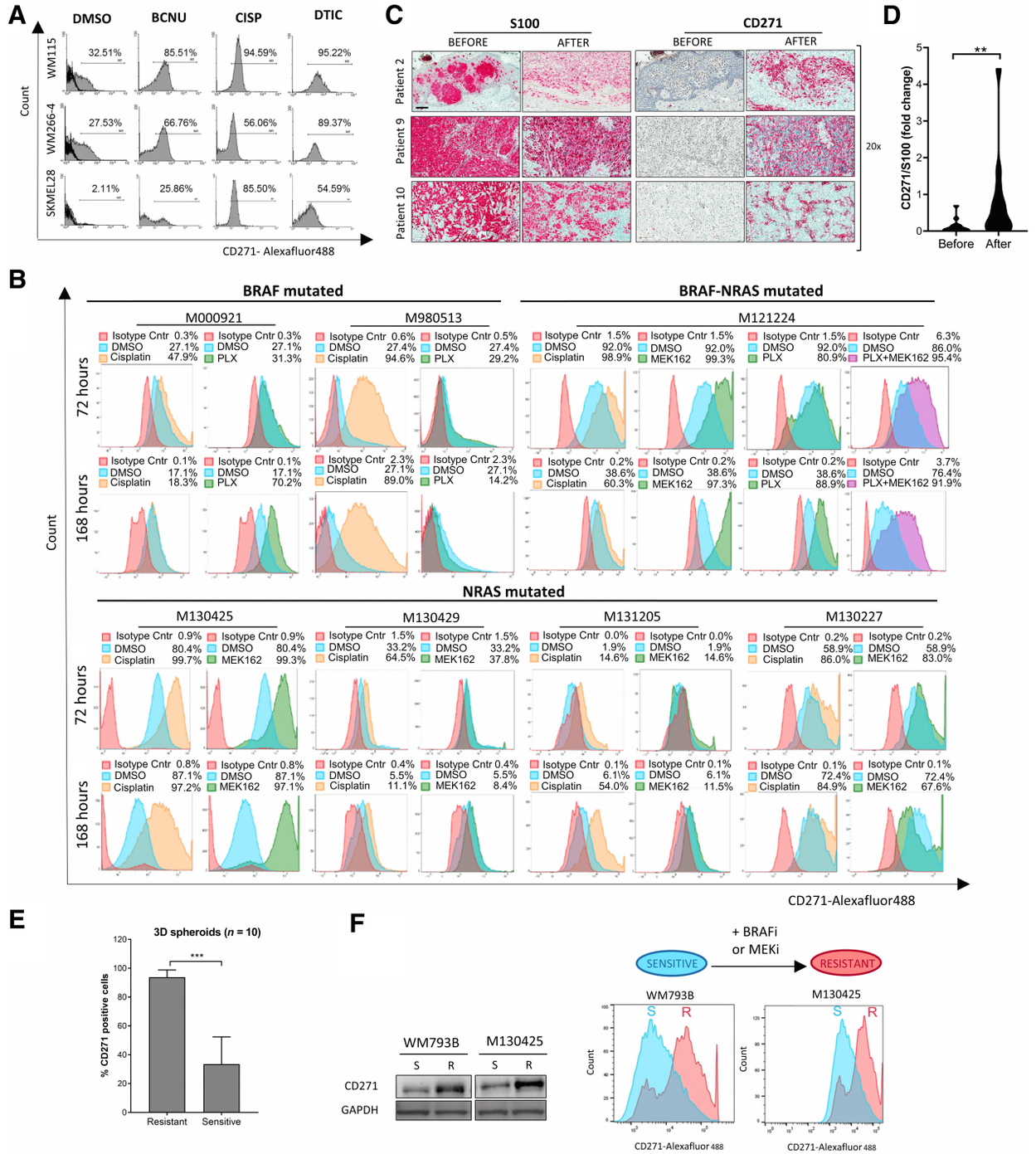

Figure 1.

CD271 is upregulated by chemo- and MAPKi therapy. **A,** Melanoma cell lines were treated with carmustine (BCNU), cisplatin (CISP), and dacarbazine (DTIC) and CD271 expression was evaluated 48 hours later by FACS. **B,** Melanoma patient–derived cells were treated with cisplatin, PLX4032 (BRAFi), and/or MEK162 (MEKi). CD271 levels were analyzed by FACS 72 and 168 hours later. **C,** Paraffin blocks derived from 13 patients were collected before and after treatment with BRAFi + MEKi and stained with S100 and CD271 Abs. Scale bar, 100 μm. **D,** Quantification of melanoma CD271+ cells was performed by QuPath. The average of 10 areas was calculated and normalized to S100. Wilcoxon matched-pairs signed rank test was used (**, $P < 0.01$). **E,** Melanoma cells were cultured in 3D for 72 hours. Spheroids were treated with trypsin to obtain a single cell suspension and CD271 expression was evaluated by FACS. **F,** BRAF (WM793B) and NRAS (M130425) mutated targeted therapy sensitive (S) cell lines were cultured with increasing concentration of BRAFi or MEKi to make the cells resistant (R) *in vitro*. CD271 expression was evaluated by Western blot and FACS comparing resistant versus sensitive cells.

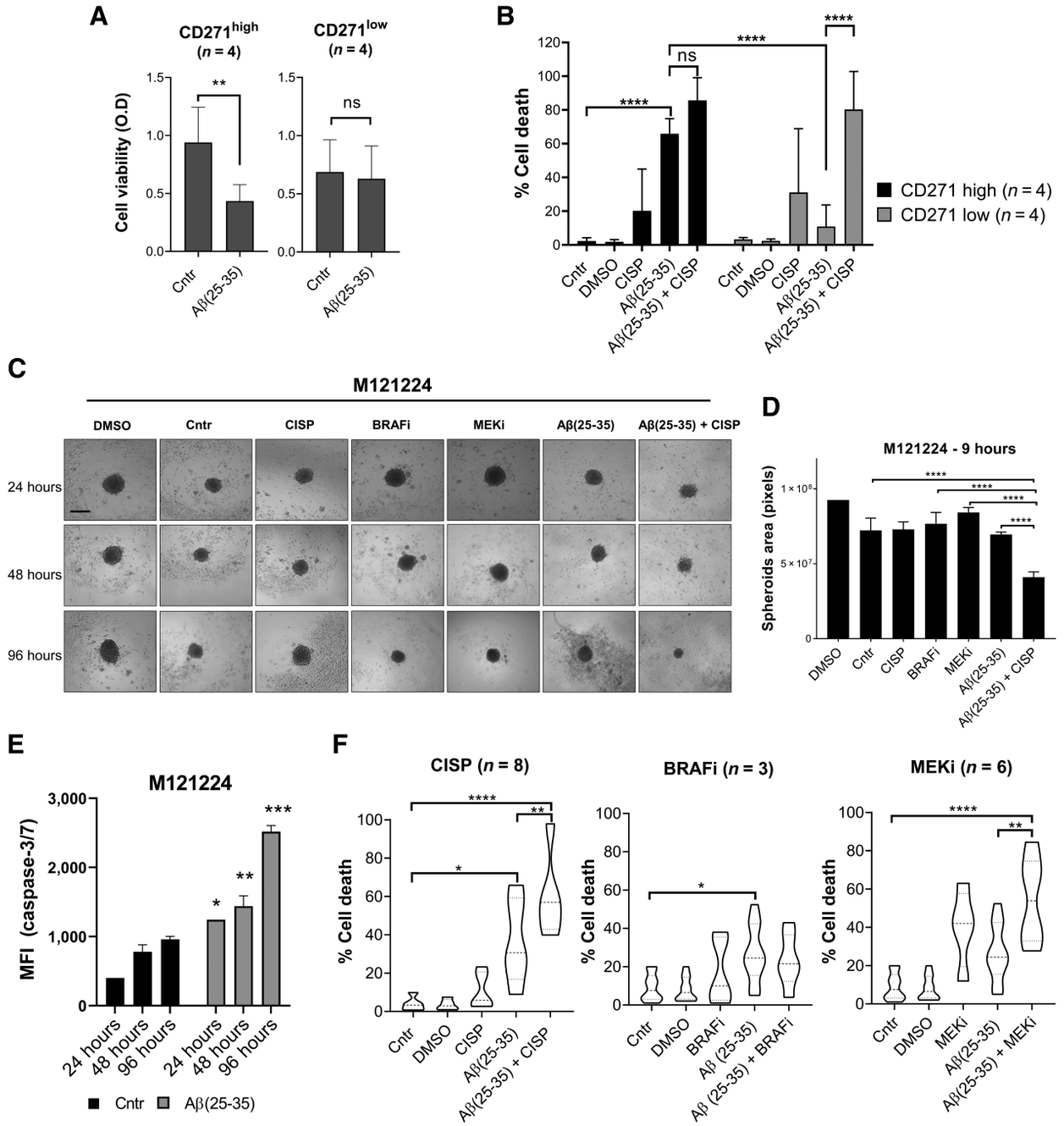

Figure 2.

$A\beta^{(25-35)}$ treatment induces cell death in melanoma 2D and 3D cultures. **A** and **B,** Eight melanoma cell lines with intrinsic $CD271^{high}$ versus $CD271^{low}$ levels were treated with $A\beta^{(25-35)}$ (40 μmol/L) alone or in combination with cisplatin (30 μmol/L). **A** and **B,** MTT assay was performed 24 hours later (**A**) and cell death (% sub-G_1; **B**) was evaluated by PI staining 72 hours after treatment. **C,** M121224 3D spheroids were treated with BRAFi (PLX4032; 3 μmol/L), MEKi (MEK162; 200 nmol/L), $A\beta^{(25-35)}$ ± cisplatin and monitored over time. Scale bar, 30 μm. **D,** Three spheroids/condition were used to measure the area with ImageJ at 96 hours from treatment. **E,** Caspase-3/7 activity was measured by FACS in M121224 spheres at different time points. **F,** 3D spheroids were treated with $A\beta^{(25-35)}$ ± cisplatin/BRAFi/MEKi. A total of 144 hours later, spheroids were stained with PI for cell death analysis by FACS. The percentage of cell death (% sub-G_1) was measured with FlowJo. Data represent the mean ± SD of triplicate determinations. *, $P < 0.05$; **, $P < 0.01$; ***, $P < 0.001$; ****, $P < 0.00001$; ns, nonsignificant.

$A\beta^{(25-35)}$ significantly reduced viability in $CD271^{high}$ cells, whereas no effect was observed in $CD271^{low}$ cells (**Fig. 2A**). However, the combination with cisplatin resulted in a strong induction of cell death in $CD271^{low}$ cells (**Fig. 2B**; Supplementary Fig. S2A). Combinations with BCNU and DTIC produced the same effect (Supplementary Figs. S2B and S2C).

To evaluate the effects of $A\beta^{(25-35)}$ on 3D spheroids, melanoma cells were seeded in agarose-coated plates and implanted into a collagen I

matrix (Supplementary Fig. S2D). M121224 spheroids, which displayed the strongest invasive capacities, showed a significant reduction in sphere area after treatment, especially in combination with cisplatin at 96 hours (**Fig. 2C** and **D**). Moreover, the evaluation of caspase-3/7 revealed the induction of apoptosis (**Fig. 2E**). Combinations with DTIC were consistent (Supplementary Fig. S2E). Cell-cycle analysis revealed that $A\beta^{(25-35)}$ significantly induced cell death in spheroids and the addition of chemo- or MAPKi showed a synergistic effect (**Fig. 2F**).

$A\beta^{(25-35)}$ reduces viability and induces death of melanoma cells in *ex vivo* patient cultures

Despite the ability of 3D spheroids to recapitulate some tumor features, they oversimplify the tumor microenvironment (23, 24). Thus, we employed *ex vivo* organotypic slice cultures. We collected fresh tumors from three patients with MAPKi-resistant, BRAF-mutated melanoma (**Fig. 3A**).

The tumors were sectioned and treated for 5 days (**Fig. 3B** and **C**; Supplementary Figs. S3A and S3B). In patient 1, $A\beta^{(25-35)}$ significantly reduced proliferating (Ki67+) cells, whereas the combination with cisplatin/BRAFi was synergistic. In patient 2, the BRAFi+MEKi failed to decrease Ki67 levels, as expected. To evaluate intrapatient variability, two different areas of the tumor were treated with Aβ (labeled as Aβ1 and Aβ2). Strikingly, the percentage of proliferating Ki67+ cells were rare with $A\beta^{(25-35)}$-treatment, which was similar in combination with cisplatin. Patient 3 confirmed these observations. Notably, the same area that was Ki67 negative was TUNEL positive, indicating apoptosis. Taken together, these data confirmed that $A\beta^{(25-35)}$ treatment induces cell death and strongly reduces melanoma proliferation in *ex vivo* models of highly resistant melanoma.

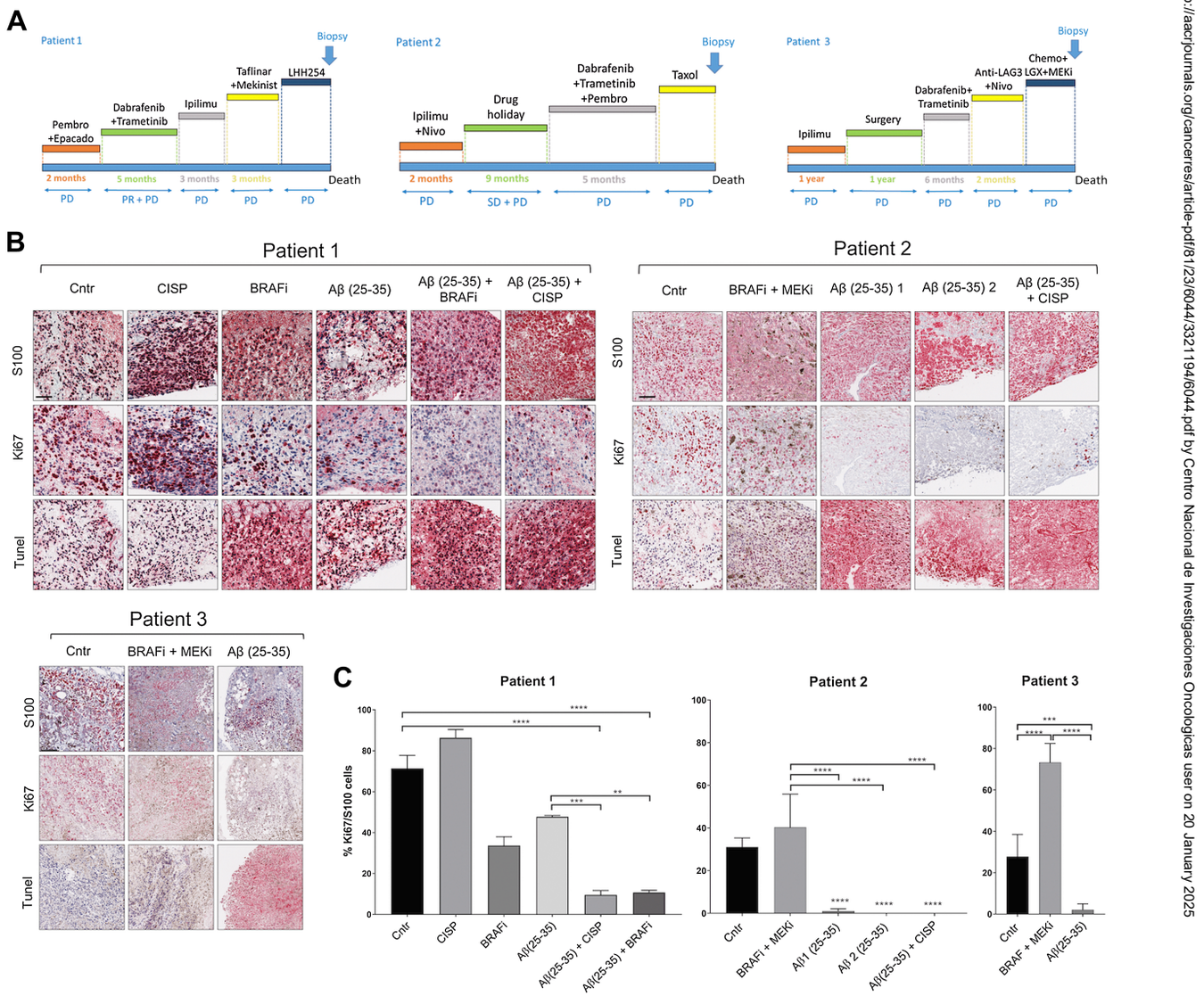

Figure 3.

$A\beta^{(25-35)}$ reduces viability and induces cell death in *ex vivo* patient cultures. **A,** Patient's treatment history. **B,** Tumor slices were cultured in the presence of different treatments for 5 days and stained with IHC. PD, progressive disease; PR, partial response; SD, stable disease. Scale bar, 100 μm. **C,** QuPath was used to quantify the number of Ki67 positive cells. The average of 10 different areas was normalized to S100. One-way ANOVA was used for statistical analysis. $^{**}P, < 0.01$; $^{***}, P < 0.001$; $^{****}, P < 0.00001$.

$A\beta^{(25-35)}$ prevents melanoma invasion in 3D cultures and metastasis formation *in vivo*

As CD271 is known to control melanoma progression (8, 11), we tested if $A\beta^{(25-35)}$ could influence melanoma invasion. Spheroids derived from MAPKi-sensitive (M980513) and resistant (M121224) cells were treated and the percentage of dead cells was assessed by live/dead staining (green/red, respectively; **Fig. 4A** and **B**). Although cisplatin had no effect on spheroid viability or invasion, $A\beta^{(25-35)}$ alone significantly increased cell death in the core of the sphere, while invading cells were alive.

Conversely, the combination of $A\beta^{(25-35)}$ with chemo- or targeted therapy induced the death of the entire sphere. Interestingly, the treatment with $A\beta^{(25-35)}$ reduced the expression of N-cadherin, Snail, and Slug and induced an increase in E-cadherin, suggesting the attenuation of the cells' invasive capacity (Supplementary Figs. S4A and S4B).

Consistently, a reduction of the area of the spheres was observed with $A\beta^{(25-35)}$+DTIC (Supplementary Fig. S4C). The percent of fragmentation (i.e., percent of invading cells outside the sphere's core) and factor shape (i.e., sphericity), two measurements correlated to increased invasion, were also significantly reduced (Supplementary Fig. S4D).

For *in vivo* validation, we generated zebrafish xenografts of human melanoma (25). We injected fluorescent human melanoma cells into the zebrafish yolk at 2 days after fertilization (2 dpf). One day after injection (1 dpi), we added chemo- or MAPKi into the water and at 2 dpi, $A\beta^{(25-35)}$ was applied. The number of fish with metastases was counted by two blinded investigators (Supplementary Fig. S4E). Notably, no *in vivo* toxicity for $A\beta^{(25-35)}$ was observed (Supplementary Fig. S4F). Strikingly, 100% of larvae injected with BRAFi-sensitive cells (M000921) were metastasis free, whereas those treated with BRAFi alone showed a higher degree of metastasis (**Fig. 4C** and **D**). Similarly, $A\beta^{(25-35)}$ alone or in combination with MEKi resulted in a significant reduction in the percentage of metastasis in MEKi-sensitive cells (M130425; **Fig. 4C** and **D**).

Finally, zebrafish injected with BRAF/NRAS-mutated MAPKi-resistant cells (M121224) showed a significant reduction in metastases with $A\beta^{(25-35)}$ alone or in combination, whereas MEKi was ineffective (**Fig. 4C** and **D**). The same reduction was observed in zebrafish treated with $A\beta^{(25-35)}$+DTIC (Supplementary Fig. S4G). Thus, these data show that $A\beta^{(25-35)}$ reduces metastases regardless of sensitivity or resistance to MAPKi (Supplementary Fig. S4H).

Moreover, $A\beta^{(25-35)}$ strongly reduces proliferation of melanoma *in vivo* and significantly reduces the expression of the invasion markers Slug/Snail (**Fig. 4E**; Supplementary Fig. S4I). Notably, a significant increase in dead cells was detected, according to caspase-3 and TUNEL staining (**Fig. 4E**; Supplementary Figs. S4J and S4K). Finally, our findings were confirmed in nude mice, revealing a significant reduction in the tumor volume and the induction of caspase-3 after 15 days of $A\beta^{(25-35)}$ monotherapy (**Fig. 4F** and **G**; Supplementary Figs. S5A–S5D).

$A\beta^{(25-35)}$-induced cell death is associated with $CD271^{high}$ expression

We next tested the selectivity of $A\beta^{(25-35)}$ for CD271 (**Fig. 5A**). Although $A\beta^{(25-35)}$ induced cell death in M130425 cells, a significant reduction was observed in CD271-KO cells (% sub-G_1: 54.8% vs. 31.6% at 2 days and 93% vs. 47.1% at 6 days in wt vs. KO, respectively; **Fig. 5B**; Supplementary Fig. S6A). Cell viability was also increased in CD271 KO cells, revealing a lower susceptibility to $A\beta^{(25-35)}$ (Supplementary Fig. S6B). To evaluate whether cell death was the result of apoptosis, we performed a double staining with PI/AnnexinV (**Fig. 5C**). Analysis of early and late apoptosis revealed a strong increase of cells undergoing apoptosis, which was significantly reduced after CD271 silencing and was confirmed in additional melanoma cells (Supplementary Figs. S6C–S6E).

We then transiently overexpressed CD271 by using a TetON lentiviral expression vector, which induces CD271 after doxycycline addition. As expected, CD271 levels increased at 48 hours in M130429 transfected cells (**Fig. 5D**) compared with empty vector (EV) control (i.e., CMVTO_EV).

Although no difference was appreciable after treatment with $A\beta^{(25-35)}$ alone, a significant increase in cell death was observed with $A\beta^{(25-35)}$+doxycycline (16.4% vs. 43.5% in CMVTO_EV vs. CMVTO_CD271, respectively; Supplementary Figs. S7A and S7B; **Fig. 5E**). Consistently, a significant reduction in viability occurred after stable CD271 overexpression (Supplementary Fig. S7C).

For further validation, M121224 cells were FACS-sorted to isolate $CD271^+$ and $CD271^-$ cells. The two subpopulations were used to generate 3D spheroids and immediately treated for 144 hours. At 24 hours, $A\beta^{(25-35)}$ prevented the formation of the sphere, giving rise to a single-cell suspension. After 144 hours of treatment, $CD271^-$ cells generated multiple spheres, whereas $CD271^+$ cells grew poorly, revealing a greater susceptibility to $A\beta^{(25-35)}$ (**Fig. 5F**). Consistently, cell death was significantly higher in $CD271^+$ than in $CD271^-$ spheres (% sub-G_1: i.e., 24 hours: 88.5% vs. 28.9%; 144 hours: 38.4% vs. 3.49%, respectively; **Fig. 5G**; Supplementary Fig. S7D). Notably, although $A\beta^{(25-35)}$ allowed $CD271^-$ cells to form multiple spheres, the addition of cisplatin prevented their growth as a consequence of CD271 upregulation (Supplementary Figs. S7E and S7F).

A further confirmation of the affinity between CD271 and $A\beta^{(25-35)}$ was demonstrated by treating the cells with $A\beta^{(25-35)}$ and a recombinant CD271 ECD soluble protein, which showed a reduction in $A\beta^{(25-35)}$ -induced cell death in a concentration dependent-manner, most likely by peptide sequestration (Supplementary Fig. S7G).

Although 100% of the M130425 wt-injected zebrafish were metastasis-free upon treatment, the percentage of metastases in CD271_KO larvae was comparable with controls, demonstrating that $A\beta^{(25-35)}$ is inefficient in the absence of the receptor also in vivo (**Fig. 5H** and **I**). We observed a reduced chance of survival in MEKi-treated fish in the presence of CD271 compared with CD271-KO. However, the addition of $A\beta^{(25-35)}$ induced a significant increase in survival probability (**Fig. 5J**).

Finally, 3D skin equivalents were generated from the same cells. Although Ki67+ was high in CD271-KO skin reconstructs after treatment, its expression was strongly reduced in those derived from control cells (Supplementary Fig. S7H).

CD271 cleavage is required to activate $A\beta^{(25-35)}$-induced apoptosis

After ligand binding, CD271 undergoes two proteolytic cleavages, with the first releasing the ECD and a carboxyl-terminal fragment (CTF). The second cleavage of CTF yields a soluble intracellular fragment (ICD). The proteolytic enzymes are the α- and γ-secretases, respectively (26). The activities of these enzymes can be suppressed by two inhibitors: the α-secretase inhibitor TAPI2, and the γ-secretase inhibitor DAPT (**Fig. 6A**). We asked whether CD271 cleavage was necessary for $A\beta^{(25-35)}$ induced apoptosis. $A\beta^{(25-35)}$ induced an initial upregulation between 16 and 24 hours, whereas at 48 hours CD271 levels gradually decreased and finally disappeared (**Fig. 6B**). Consistently, CD271 was strongly reduced 72 hours after treatment in four

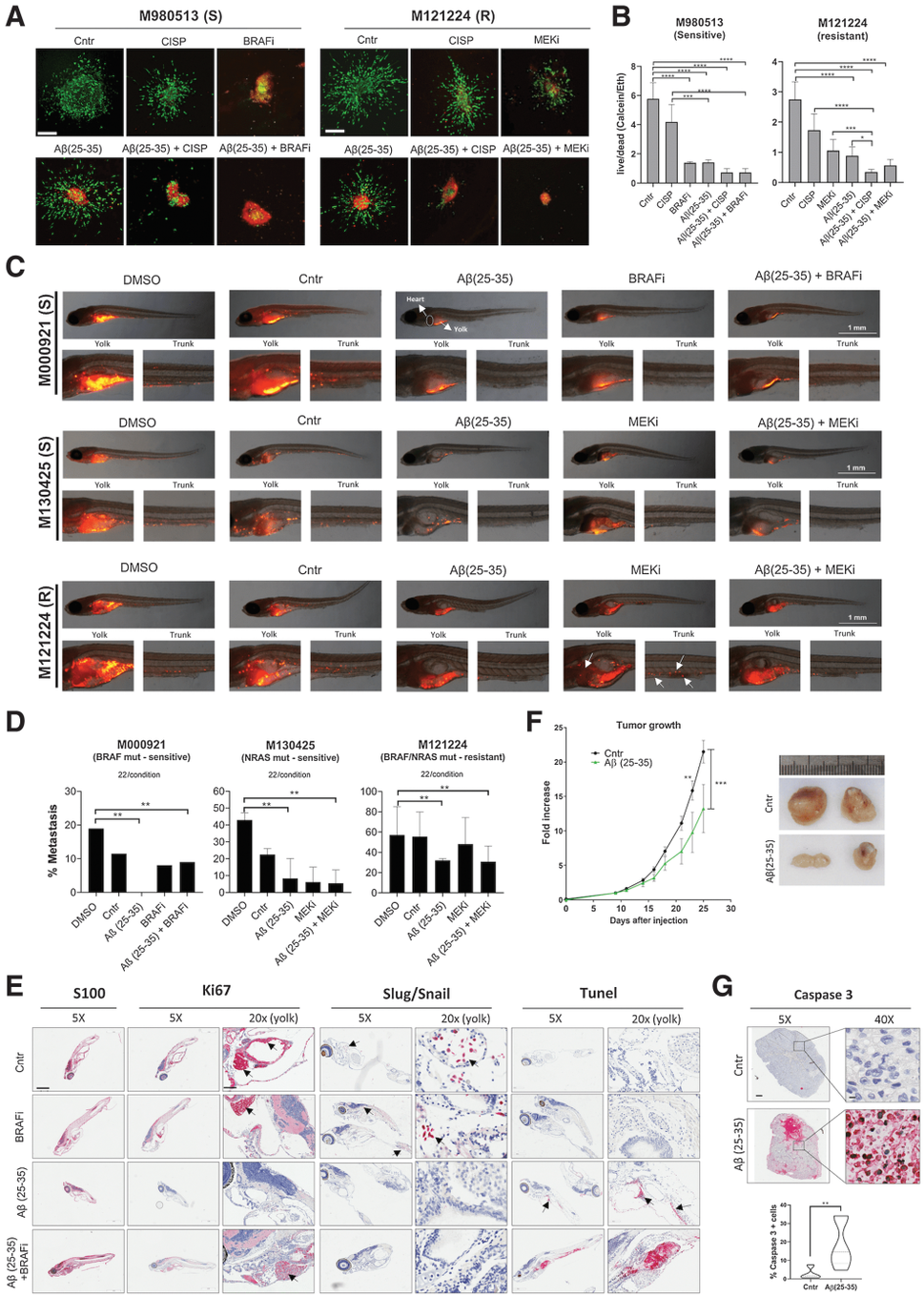

Figure 4.

$A\beta^{(25-35)}$ prevents melanoma invasion and metastasis formation *in vivo.* **A** and **B,** M980513 (S, sensitive) and M121224 (R, resistant) spheres were implanted into a matrix of collagen I and treated with $A\beta^{(25-35)}$ 40 μmol/L ± cisplatin/BRAFi/MEKi. A total of 168 hours later, spheres were stained to evaluate the live (calcein; green)/dead (ethidium; red) cells. Scale bar, 30 μm. **B,** The live/dead ratio was analyzed in six spheres/condition by Photoshop. **C,** MAPKi-sensitive and resistant melanoma cells were stained with Vibrant Dye (red) and injected into the yolk of zebrafish larvae. Twenty-four hours later, zebrafish were treated with BRAFi/MEKi and $A\beta^{(25-35)}$ was injected into the yolk the day after. Pictures were taken 4 days later and the number of zebrafish with metastasis (**D**) was evaluated by two blind investigators. Data represent the mean ± SD of two independent experiments (tot = 660). One-way ANOVA was used for statistical analysis. **, $P < 0.01$; ***, $P < 0.001$. **E,** M000921-injected zebrafish were stained with S100, Ki67, Slug/Snail, and TUNEL. Scale bar, 500 μm (5×) and 100 μm (20×). **F,** A total of 500000 M121224 cells were subcutaneously injected in 9-weeks-old female nude mice. When tumor reached approximately 50 mm^3, BSA or 15 μg $A\beta^{(25-35)}$ was intratumorally injected three times a week. Tumor growth was measured using an electronic caliper. Mice were sacrificed when control tumors reached 1,000 m^3. Fold increase was calculated using each individual measure at day 7 to standardize. Representative images are shown (n = 5–8 tumors/group. **G,** Caspase-3 staining was performed on six tumors/group and quantified by QuPath. Scale bar, 4 mm (5×) and 200 μm (40×). Two-way Anova; **, $P \leq 0.01$.

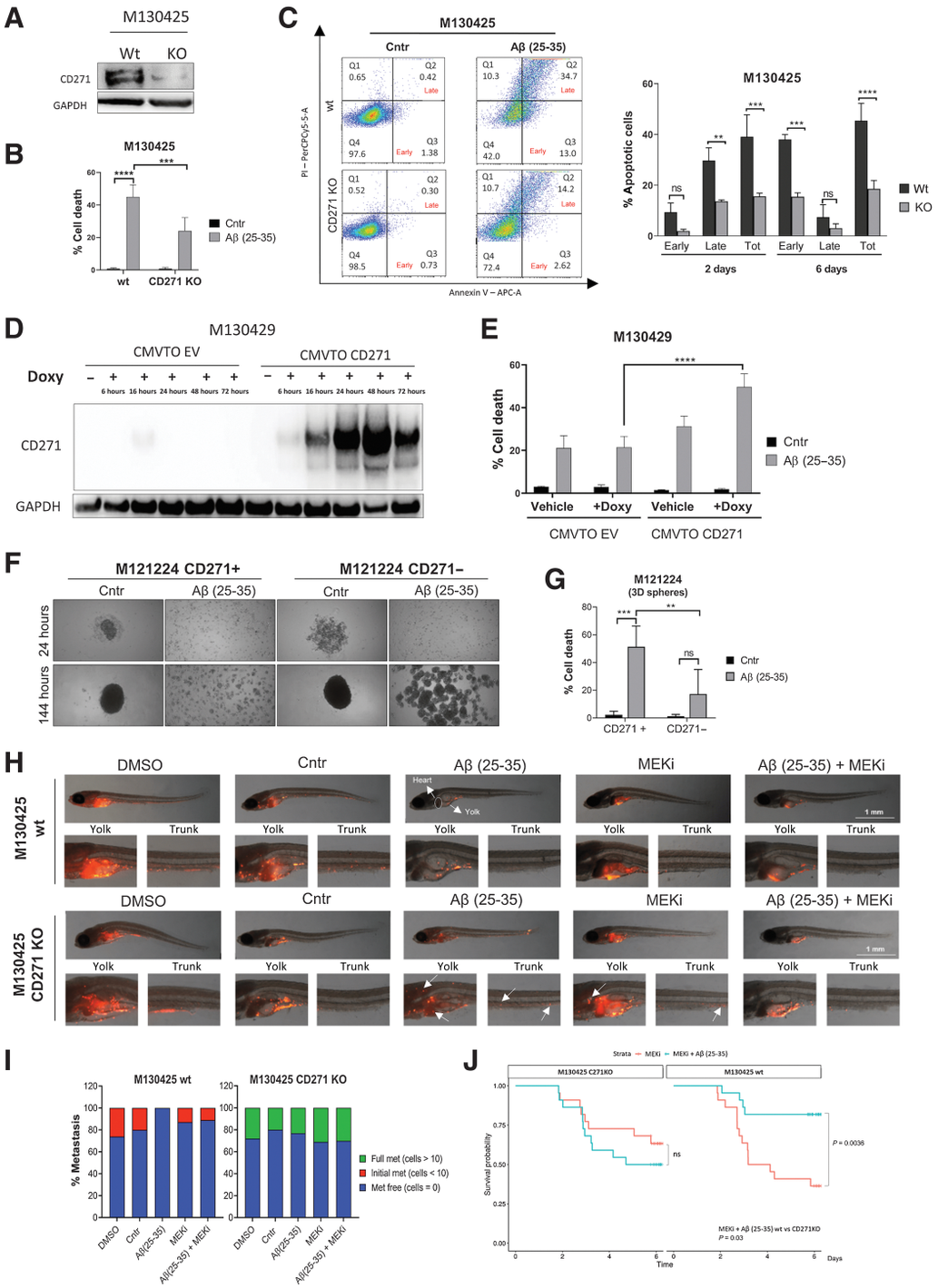

Figure 5.

CD271^{high} cells display a greater susceptibility to Aβ$^{(25–35)}$-induced death. **A,** CD271 silencing was confirmed by Western blot. **B,** Melanoma cells were treated with Aβ$^{(25–35)}$ 40 μmol/L and the amount of dead cells (% sub-G_1) was measured by PI staining at the FACS. **C,** AnnexinV/PI assay was performed to evaluate the percentage of early and late apoptotic cells. **D,** CMVTO_EV- and CMVTO_CD271-transfected cells were treated with doxycycline, and proteins were collected to evaluate CD271 induction by Western blot. **E,** Melanoma cells were treated with doxycycline for 48 hours, followed by Aβ$^{(25–35)}$ administration. PI staining was performed 24 hours later and the percentage of dead cells was measured by FACS. **F,** M121224 CD271+ and − cells were seeded as spheroids and treated with Aβ$^{(25–35)}$. Twenty-four and 144 hours later, brightfield pictures were taken and PI staining (**G**) was performed. Data represent the mean ± SD of triplicate determinations. **H,** M130425 wt and CD271 KO cells were injected into the yolk of zebrafish larvae and treated with Aβ$^{(25–35)}$ ± MEKi. Pictures of wt are the same of **Fig. 4C**. **I,** The severity of metastasis was evaluated 4 days later by two blind investigators. **J,** Probability of survival in zebrafish injected with wt versus CD271 KO cells. Two-way ANOVA was used for statistical analysis. **, $P < 0.01$; ***, $P < 0.001$; ****, $P < 0.00001$; ns, nonsignificant.

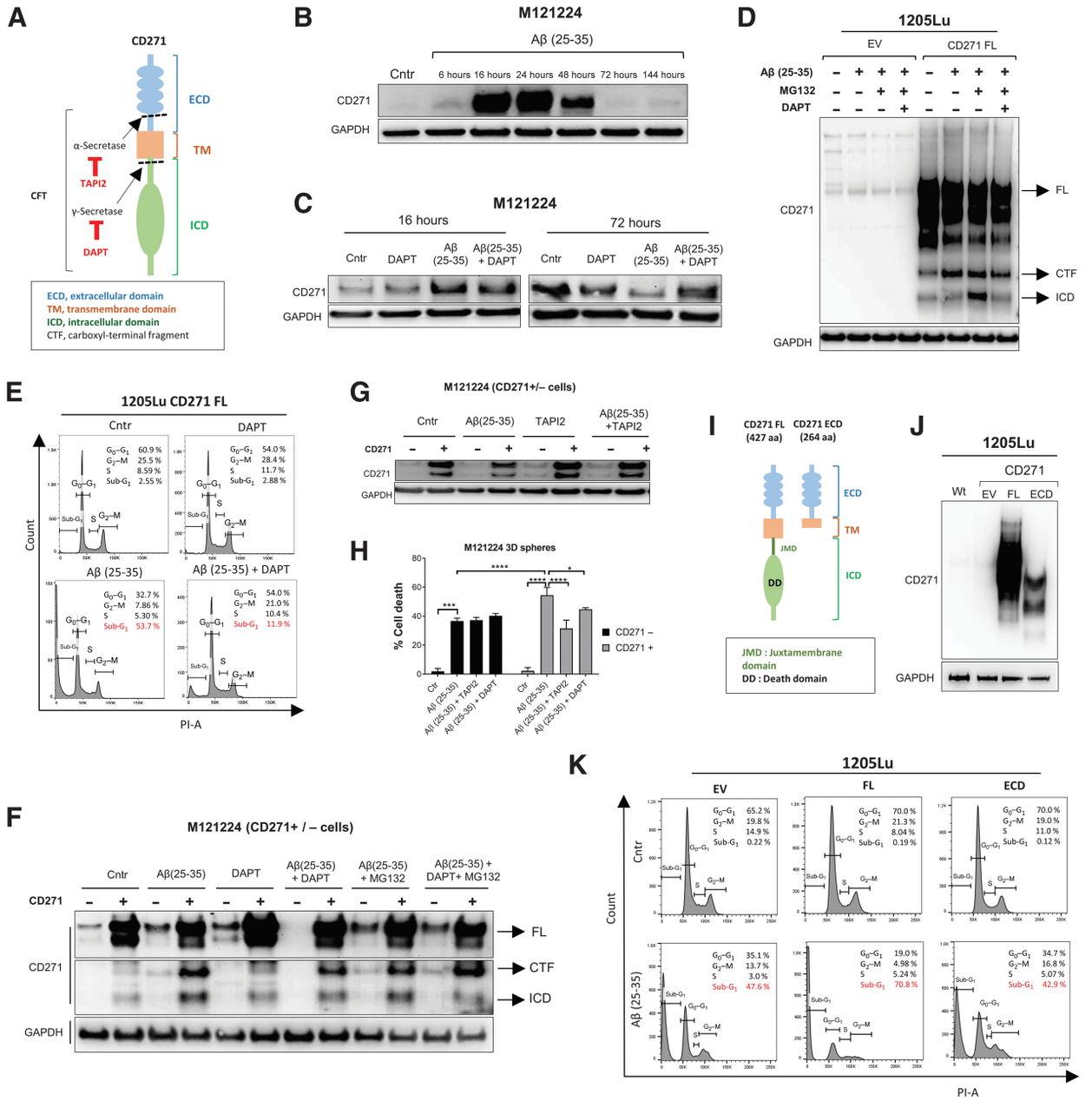

Figure 6.

CD271 cleavage is required to activate $A\beta^{(25-35)}$-induced apoptosis. **A,** Representation of CD271 cleavage sites and the inhibitors used. **B,** CD271 levels were evaluated by Western blot after treatment with $A\beta^{(25-35)}$ at different time points. **C,** M121224 cells were seeded in six-well plates and treated with $A\beta^{(25-35)}$ 40 μmol/L ± DAPT (200 nmol/L) for 16 and 72 hours. Protein extracts were immunoblotted with CD271. **D,** 1205Lu CD271 EV and FL (full length) cells were pretreated with MG132 (20 μmol/L) + DAPT (300 nmol/L) for 1 hour. CTF and ICD formation was evaluated by Western blot. **E–G,** 1205Lu FL cells were treated for 1 hour with DAPT (300 nmol/L; **E**), then $A\beta^{(25-35)}$ 40 μmol/L was added in the medium for 30 minutes and PI staining was performed CD271 + and − sorted cells were treated with $A\beta^{(25-35)}$ ± DAPT (300 nmol/L)/MG132 (20 μmol/L)/TAPI2 (500 nmol/L; **F** and **G**). CD271 was evaluated by Western blot. **H,** Cell cycle by FACS. Two-way ANOVA was used for statistical analysis. *, $P < 0.05$; ***, $P < 0.001$; ****, $P < 0.00001$. **I,** CD271 FL and ECD structure. **J,** 1205Lu wt, EV, FL, and ECD lysates were immunoblotted for CD271 Ab. **K,** Melanoma cells were treated for 1 hour with $A\beta^{(25-35)}$ (40 μmol/L) and stained with PI for cell-cycle evaluation by FACS.

different cell lines (Supplementary Fig. S8A). We hypothesized that this reduction was due to the cleavage and the consequent degradation into the proteasome. To test this hypothesis, cells were treated with $A\beta^{(25-35)}$ with DAPT (**Fig. 6C**). Although no difference was observed at 16 hours, likely because the receptor activation had not yet occurred, the prolonged treatment for 72 hours with $A\beta^{(25-35)}$+DAPT prevented CD271 cleavage and its subsequent degradation (**Fig. 6C**).

To confirm this, we overexpressed CD271 in 1205Lu cells and we evaluated its cleavage by using an antibody that detects the ICD (**Fig. 6D**). The treatment of 1205Lu CD271_FL cells with $A\beta^{(25-35)}$

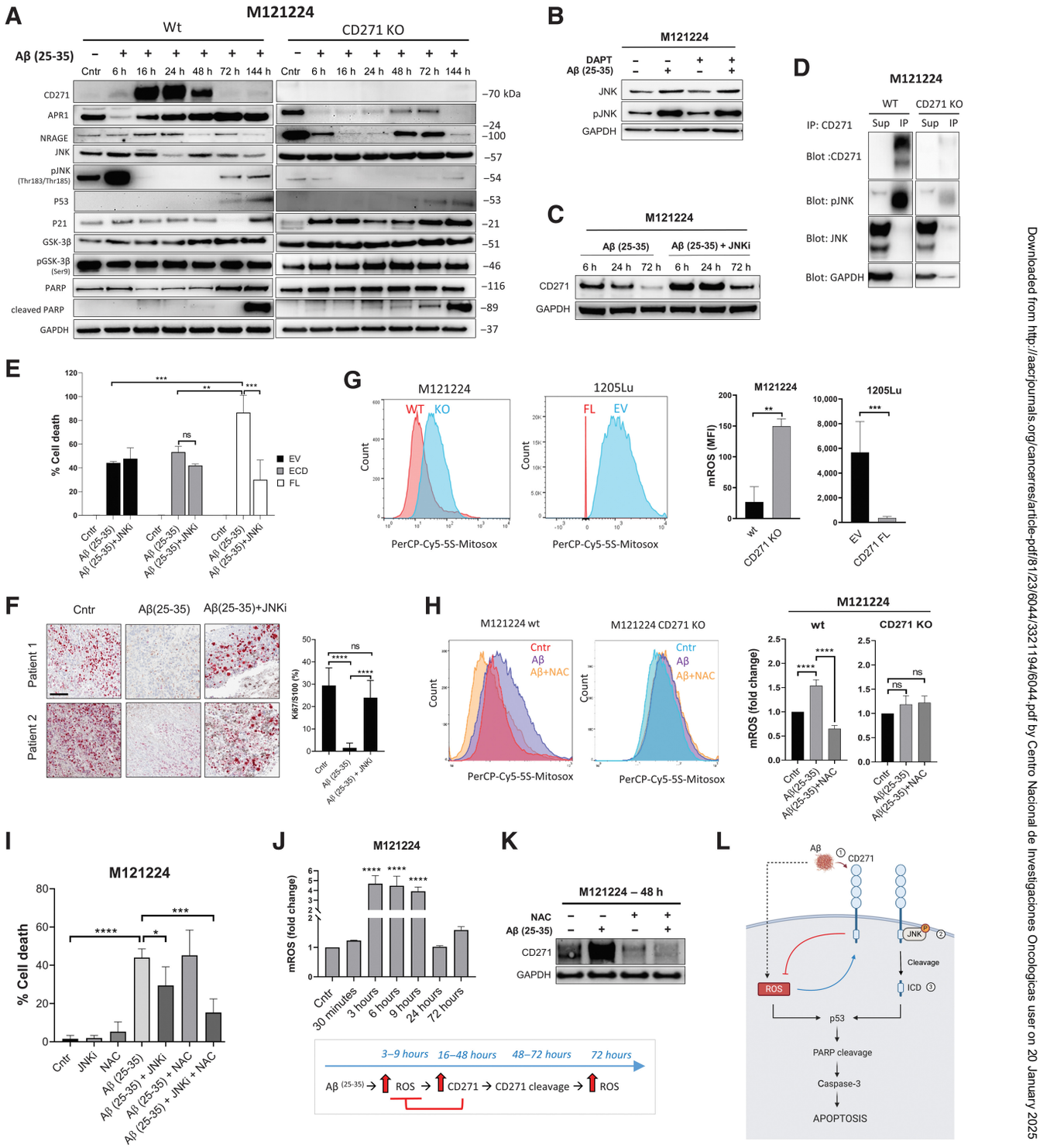

Figure 7.

Melanoma cell death is triggered by $A\beta^{(25-35)}$-mediated activation of CD271–JNK pathway and mitochondrial ROS production. **A,** Western blot on melanoma cells were treated with $A\beta^{(25-35)}$ (40 μmol/L) at different time points. CD271 and GAPDH belong to the same Western blot shown in **Fig. 6B**. **B** and **C,** M121224 wt cells were treated with $A\beta^{(25-35)}$ (40 μmol/L) ± DAPT (200 nmol/L) or JNKi (SP600125; 300 nmol/L) and Western blot was performed. **D,** M121224 wt and CD271 KO cells were treated for 48 hours with $A\beta^{(25-35)}$ (40 μmol/L). Lysates were pulled-down with CD271 Ab, and supernatant (Sup) and immunoprecipitates (IP) were immunoblotted with different Abs. **E,** Melanoma cells were treated with $A\beta^{(25-35)}$ (40 μmol/L) ± JNKi (SP600125; 200 nmol/L) for 1 hour and stained with PI. The percentage of cell death was evaluated by FACS. Two-way ANOVA was used for statistical analysis. **, $P < 0.01$; ***, $P < 0.001$. (*Continued on the following page.*)

and the proteasome inhibitor MG132 allowed the detection of both CTF and ICD fragments (**Fig. 6D**). No cleavage was detectable in the absence of $A\beta^{(25-35)}$. Notably, the addition of DAPT prevented the formation of the ICD and strongly decreased apoptosis in CD271_FL cells (**Fig. 6D** and **E**).

The same finding was confirmed in M121224 cells (Supplementary Fig. S8B). Treatment with TAPI2/DAPT in $CD271^+$ cells prevented the cleavage (**Fig. 6F** and **G**). Consistently, cell death rescue was observed in $CD271^+$ spheres after treatment with $A\beta^{(25-35)}$+DAPT/TAPI2, whereas no difference was appreciable in the $CD271^-$ spheres (**Fig. 6H**).

To evaluate if the ICD is necessary for the activation of apoptosis, we overexpressed a truncated form of the receptor containing only the ECD (**Fig. 6I** and **J**). Interestingly, the percentage of cell death after treatment was dramatically reduced from 70.8% (FL) to 42.9% (ECD), being comparable with the EV (**Fig. 6K**). Taken together, these data strongly suggest that $A\beta^{(25-35)}$ activates CD271 cleavage and that the ICD is necessary for mediating apoptotic cell death.

Melanoma cell death is triggered by activation of CD271–JNK pathway and mitochondrial ROS production

To investigate the mechanisms involved in Aβ-CD271 apoptosis, we evaluated the expression of known CD271 interactors (**Fig. 7A**; refs. 27–29). APR1 increased over time, whereas JNK was strongly phosphorylated at 6 hours only in wt but not in CD271_KO cells. Interestingly, the highest APR1 expression occurred at 72 hours, when CD271 was downregulated (Supplementary Fig. S8C). To verify the involvement of APR1, the protein was silenced in M121224 cells. However, APR1 silencing did not significantly decrease death compared with controls (Supplementary Fig. S8D). Thus, we asked whether the phosphorylation of JNK was affected by CD271 activation. We treated cells with $A\beta^{(25-35)}$+DAPT observing no difference in JNK phosphorylation, suggesting activation upstream of CD271 cleavage (**Fig. 7B**). To test this hypothesis, we treated the cells with $A\beta^{(25-35)}$ in the presence of the pJNK inhibitor (SP600125) and we observed CD271 rescue in comparison to $A\beta^{(25-35)}$ alone, confirming a delayed cleavage (**Fig. 7C**). Moreover, a CD271 co-immunoprecipitation assay revealed a direct interaction with pJNK (**Fig. 7D**). The JNKi rescued only 1205Lu_FL cells, whereas the treatment was ineffective in 1205Lu_ECD cells, demonstrating the role of JNK in inducing apoptosis through the generation of ICD (**Fig. 7E**). Moreover, the inhibition of pJNK in *ex vivo* melanoma slices rendered the treatment ineffective (**Fig. 7F**).

It has been shown that Aβ impairs the mitochondrial redox activity, leading to ROS formation and cell death (30, 31). To verify whether mitochondrial ROS (mROS) were also involved in $A\beta^{(25-35)}$-mediated apoptosis, we evaluated their levels in the presence/absence of CD271 (**Fig. 7G**). Interestingly, mROS strongly increased after CD271 silencing in M121224, whereas its overexpression in 1205Lu cells significantly reduced mROS levels (**Fig. 7G**). These data revealed an unexpected role of CD271 as a mROS inhibitor. The same result was observed in 1205Lu ECD transfected cells, showing that CD271-mediated ROS inhibition does not require its ICD (Supplementary Fig. S8E). Consistently, the treatment with doxycycline to induce CD271 strongly reduced ROS compared with control (Supplementary Fig. S8E). Despite its function as a ROS scavenger, the treatment with $A\beta^{(25-35)}$ for 72 hours induced a significant upregulation of mROS in control but not in KO cells, revealing their production to be CD271-dependent (**Fig. 7H**). Moreover, this induction was reverted in the presence of the scavenger N-acetylcysteine (NAC; **Fig. 7H**; Supplementary Fig. S8F). These results were confirmed in 1205Lu cells (Supplementary Fig. S8G).

$A\beta^{(25-S35)}$ treatment with JNKi+NAC significantly reduced cell death, showing a synergistic effect and demonstrating the co-existence of two apoptotic pathways: (i) a pJNK-CD271 cleavage pathway; and (ii) a mROS pathway, both dependent on the presence of CD271 (**Fig. 7I**).

To better understand the kinetics of ROS production, we treated M121224 cells and analyzed ROS levels over time: before CD271 upregulation (0–16 hours), during its induction (16–24 hours), and after cleavage (48–72 hours; **Fig. 7J**). Interestingly, mROS significantly increased between 3 and 9 hours. However, at 24 hours, when CD271 upregulation was maximal, mROS returns to the basal levels confirming its inhibitory role. Finally, after its cleavage, the levels begin rising, presumably as a consequence of the lack of CD271 (**Fig. 7J**). Interestingly, the upregulation of CD271 between 24 and 48 hours was prevented by NAC (**Fig. 7K**). These results show that $A\beta^{(25-35)}$ cell death is triggered by the activation of the CD271–JNK–ROS pathway. Moreover, we discovered a feedback loop in which mROS induces CD271 upregulation, which acts as a ROS scavenger (**Fig. 7L**).

Finally, to evaluate the induction of apoptosis, PARP cleavage and activation of p53 were also detected (**Fig. 7A**). Surprisingly, p53 and PARP were activated also in CD271_KO cells as well as in the presence of DAPT and in $CD271^{low}$ cells (**Fig. 7A**; Supplementary Figs. S8H–S8J), suggesting the presence of a CD271-independent pathway. In line with this assumption, caspase-3/7 activation in CD271_KO cells revealed the existence of an alternative mechanism (Supplementary Fig. S8K). In addition, immunofluorescence showed that $A\beta^{(25-35)}$ can enter the cells and accumulate preferentially in the cytoplasm of $CD271^{low}$ cells, whereas it localizes at the membrane in the presence of the receptor (Supplementary Fig. S8L).

Discussion

Despite data demonstrating a role for CD271 in melanoma, few studies go beyond merely describing it as a biomarker. The pathways modulated by CD271 in melanoma, and the possibility of activating CD271 with specific ligands has been poorly explored.

In this study, we observed a significant induction of CD271 following different treatments, which makes CD271 an attractive therapeutic target. Ngo and coworkers conjugated an anti-CD271 antibody with saporin to kill CD271-expressing cells (32). Although the combination of an anti-CD47 Ab+CD271-saporin Ab in mice significantly reduced the volume of primary tumors, the treatment with CD271-

(*Continued.*) **F,** Tumor slices were treated for 5 days and stained with Ki67 and S100 Abs. Ki67+ cells were quantified by QuPath. The average of 10 areas was normalized to the total S100. Two-way ANOVA was used for statistical analysis. ****, $P < 0.00001$. Scale bar, 100 μm. "Cntr" are the same pictures shown also in **Fig. 3** (patient 2 and 3). **G,** Cells were stained with MitoSOX (5 μmol/L) and the levels of mROS were measured by FACS. Data represent the mean ± SD of triplicate determinations. One-way ANOVA was used for statistical analysis. **, $P < 0.01$; ***, $P < 0.001$. **H,** Melanoma cells were treated with $A\beta^{(25-35)}$ (40 μmol/L) ± NAC (5 mmol/L) for 72 hours and stained with MitoSOX. mROS were measured by FACS. **I,** M121224 were treated with $A\beta^{(25-35)}$ alone or in combination with JNKi (200 nmol/L) ± NAC (5 mmol/L). Cells were stained with PI and the percentage of cell death was evaluated by FACS. One-way ANOVA was used for statistical analysis. *, $P < 0.05$; ***, $P < 0.001$; ****, $P < 0.00001$. **J,** M121224 cells were treated with $A\beta^{(25-35)}$ and mROS were measured by FACS at different time points. **K,** M121224 CD271+ cells were treated with $A\beta^{(25-35)}$ (40 μmol/L) ± NAC (5 mmol/L) for 48 hours. CD271 levels were evaluated by Western blot. **L,** Graphical representation of CD271–JNK–ROS pathway induced following $A\beta^{(25-35)}$ treatment. ns, nonsignificant.

saporin Ab alone was ineffective. However, it strongly reduced the percentage of metastases. These data highlight the necessity of activating CD271 to induce apoptosis.

In contrast, other studies attempted to target CD271 by inhibiting its upstream regulators. Mohammad and colleagues used vemurafenib with cJun/FAK/Scr inhibitors, thus preventing CD271 upregulation (5). Similarly, Rambow and colleagues used a RXRγ antagonist, observing a significant reduction in $CD271^{high}$ cell accumulation (12).

In contrast to these approaches, we exploited the high CD271 levels induced by therapies to activate ligand-specific receptor cleavage and apoptosis by using a 10-amino-acid $A\beta^{(25-35)}$ peptide *in vitro*, *ex vivo*, and *in vivo*.

We demonstrated that $A\beta^{(25-35)}$ significantly induced apoptosis, and reduced metastasis *in vivo* in a CD271-dependant manner. $A\beta^{(25-35)}$ induced CD271 cleavage, releasing the ICD death domain, which mediates apoptosis. A γ-secretase inhibitor prevented CD271 cleavage, significantly rescuing peptide-treated cells. Consistently, several studies showed that mutations in the ICD prevent cell death (33).

After recruiting its cytosolic interactors, CD271 mediates JNK phosphorylation, which in turn induces the α-secretase TACE/ADAM17, leading to CD271 cleavage (34, 35). Here, we demonstrate that JNK phosphorylation was necessary for the generation of the ICD and that CD271 and pJNK directly interact. Pharmacologic inhibition of JNK not only delayed CD271 cleavage, but also significantly reduced treatment efficacy.

The role of JNK in β-amyloid–induced death was also previously shown in a neuroblastoma cell line (35). Specifically, β-amyloid induced death by activating p38 and JNK kinases in an ICD-dependent manner. Interestingly, JNK was not phosphorylated in CD271_KO cells, demonstrating the pathway to be receptor-dependent.

β-Amyloid generates pores in the mitochondrial membrane, leading to cytochrome c release (36). Moreover, β-amyloid can directly inhibit ATP production, altering the enzymatic mitochondrial machinery and inducing a strong production of ROS (37).

We showed that CD271 silencing induced mROS production 1,000-fold. Moreover, the pharmacologic inhibition of both pathways (i.e., JNK and ROS) demonstrated a synergistic effect by rescuing the cells from apoptosis and demonstrating the presence of two CD271-apoptotic pathways.

These findings highlight a role for CD271 in ROS inhibition. Indeed, although $CD271^{low}$ cells treated with a BRAFi upregulate mROS, CD271 overexpression prevents ROS induction (Supplementary Fig. S8M). Despite these results, further studies are needed to understand to what degree this can abrogate the cell killing effect of MAPK inhibitors.

In conclusion, we revealed that ligand-mediated CD271 cleavage induces apoptosis in melanoma by releasing its ICD and preventing metastasis *in vivo*. Although this demonstrates the potential efficacy of CD271 targeting *in vivo*, the ability of the ECD to sequester $A\beta^{(25-35)}$, and thereby attenuate this affect should be studied further for clinical application. However, amyloids have been used in patients successfully. Amyloid-peptides conjugated with a cell penetrating peptide showed a selective killing of cancer cells without toxicity in healthy cells (38). In addition, previous studies suggest amyloids in the formulation of long-acting drugs (GnRH analogs Degarelix and Antagon) for the treatment of prostate cancer and in assisted reproduction, respectively (39). Both drugs are in phase III clinical trials and showed a good safety margin. Thus, understanding the interaction between the $A\beta^{(25-35)}$ peptide and CD271_ECD will facilitate developing drugs that mimic the effect of amyloid without toxicity.

Authors' Disclosures

N. Tiso reports grants from AIRC and Italian Telethon during the conduct of the study and grants from AIRC and Italian Telethon outside the submitted work. R. Dummer reports personal fees from Novartis, Merck Sharp & Dhome, Bristol-Myers Squibb, Roche, Amgen, Takeda, Pierre Fabre, Sun Pharma, Sanofi, Catalym, Second Genome, Regeneron, Alligator, T3 Pharma, MaxiVAX SA, Pfizer, and touchIME outside the submitted work. M.P. Levesque reports project focused research funding from Roche, Novartis, Molecular Partners, and Oncobit AG. No disclosures were reported by the other authors.

Authors' Contributions

A. Saltari: Conceptualization, data curation, formal analysis, funding acquisition, validation, methodology, writing–original draft, project administration, writing–review and editing. **A. Dzung:** Formal analysis, validation, methodology. **M. Quadri:** Data curation, validation, investigation, visualization, methodology. **N. Tiso:** Resources, funding acquisition, investigation, visualization, methodology, writing–review and editing. **N. Facchinello:** Formal analysis, validation, methodology. **A. Hernández-Barranco:** Data curation, validation, investigation, visualization. **S. Garcia-Silva:** Data curation, formal analysis, validation, visualization, methodology. **L. Nogués:** Validation, methodology. **C.I. Stoffel:** Validation, visualization, methodology. **P.F. Cheng:** Software, formal analysis. **P. Turko:** Software, formal analysis. **O.M. Eichhoff:** Conceptualization, supervision. **F. Truzzi:** Conceptualization, data curation, supervision. **A. Marconi:** Resources, supervision, funding acquisition. **C. Pincelli:** Conceptualization, funding acquisition, writing–review and editing. **H. Peinado:** Conceptualization, methodology. **R. Dummer:** Conceptualization, resources, funding acquisition. **M.P. Levesque:** Conceptualization, resources, supervision, writing–original draft, writing–review and editing.

Acknowledgments

The authors thank Prof. Lukas Sommer and Dr. Gaetana Restivo for helping with cloning and Melanie Maudrich and Federica Sella for all their valuable help. This work was supported by the FIRC grant 2015 18145 (to A. Saltari), AIRC grant IG 2017 19928 (to N. Tiso), and the Telethon grant GGP19287 (to N. Facchinello). N. Facchinello is a fellow of the Umberto Veronesi Foundation.

The publication costs of this article were defrayed in part by the payment of publication fees. Therefore, and solely to indicate this fact, this article is hereby marked "advertisement" in accordance with 18 USC section 1734.

Note

Supplementary data for this article are available at Cancer Research Online (http://cancerres.aacrjournals.org/).

Received January 29, 2021; revised July 20, 2021; accepted October 11, 2021; published first October 13, 2021.

References

1. Nishimura EK, Jordan SA, Oshima H, Yoshida H, Osawa M, Moriyama M, et al. Dominant role of the niche in melanocyte stem-cell fate determination. Nature 2002;416:854–60.
2. Boiko AD, Razorenova OV, van de Rijn M, Swetter SM, Johnson DL, Ly DP, et al. Human melanoma-initiating cells express neural crest nerve growth factor receptor CD271. Nature 2010;466:133–7.
3. Cheli Y, Bonnazi VF, Jacquel A, Allegra M, De Donatis GM, Bahadoran P, et al. CD271 is an imperfect marker for melanoma initiating cells. Oncotarget 2014;5:5272–83.
4. Lehraiki A, Cerezo M, Rouaud F, Abbe P, Allegra M, Kluza J, et al. Increased CD271 expression by the NF-kB pathway promotes melanoma cell survival and drives acquired resistance to BRAF inhibitor vemurafenib. Cell Discov 2015;1:15030.

5. Fallahi-Sichani M, Becker V, Izar B, Baker GJ, Lin JR, Boswell SA, et al. Adaptive resistance of melanoma cells to RAF inhibition via reversible induction of a slowly dividing de-differentiated state. Mol Syst Biol 2017;13:905.
6. Pincelli C. p75 neurotrophin receptor in the skin: beyond its neurotrophic function. Front Med 2017;4:22.
7. Truzzi F, Marconi A, Lotti R, Dallaglio K, French LE, Hempstead BL, et al. Neurotrophins and their receptors stimulate melanoma cell proliferation and migration. J Invest Dermatol 2008;128:2031–40.
8. Restivo G, Diener J, Cheng PF, Kiowski G, Bonalli M, Biedermann T, et al. The low neurotrophin receptor CD271 regulates phenotype switching in melanoma. Nat Commun 2018;9:314.
9. Behrens MI, Lendon C, Roe CM. A common biological mechanism in cancer and Alzheimer's disease? Curr Alzheimer Res 2009;6:196–204.
10. Radke J, Roßner F, Redmer T. CD271 determines migratory properties of melanoma cells. Sci Rep 2017;7:9834.
11. Saltari A, Truzzi F, Quadri M, Lotti R, Palazzo E, Grisendi G. CD271 down-regulation promotes melanoma progression and invasion in three-dimensional models and in zebrafish. J Invest Dermatol 2016;136:2049–58.
12. Rambow F, Rogiers A, Marin-Bejar O, Aibar S, Femel J, Dewaele M, et al. Toward minimal residual disease-directed therapy in melanoma. Cell 2018; 174:843–55.
13. Li S, Yue D, Chen X, Wang L, Li J, Ping Y, et al. Epigenetic regulation of CD271, a potential cancer stem cell marker associated with chemoresistance and metastatic capacity. Oncol Rep 2015;33:425–32.
14. Redmer T, Walz I, Klinger B, Khouja S, Welte Y, Schäfer R, et al. The role of the cancer stem cell marker CD271 in DNA damage response and drug resistance of melanoma cells. Oncogenesis 2017;6:e291.
15. Zhou X, Hao Q, Liao P, Luo S, Zhang M, Hu G, et al. Nerve growth factor receptor negates the tumor suppressor p53 as a feedback regulator. Elife 2016; 5:e15099.
16. Yaar M, Zhai S, Pilch PF, Doyle SM, Eisenhauer PB, Fine RE, et al. Binding of beta-amyloid to the p75 neurotrophin receptor induces apoptosis. A possible mechanism for Alzheimer's disease. J Clin Invest 1997;100:2333–40.
17. Costantini C, Rossi F, Formaggio E, Bernardoni R, Cecconi D, Della-Bianca V. Characterization of the signaling pathway downstream p75 neurotrophin receptor involved in beta-amyloid peptide-dependent cell death. J Mol Neurosci 2005; 25:141–56.
18. Sotthibundhu A, Sykes AM, Fox B, Underwood CK, Thangnipon W, Coulson EJ. Beta-amyloid (1-42) induces neuronal death through the p75 neurotrophin receptor. J Neurosci 2008;28:3941–6.
19. Devarajan S, Sharmila JS. Computational studies of beta amyloid (Aβ42) with p75NTR receptor: a novel therapeutic target in Alzheimer's disease. Adv Bioinformatics 2014;2014:736378.
20. Perini G, Della-Bianca V, Politi V, Della Valle G, Dal-Pra I, Rossi F, et al. Role of p75 neurotrophin receptor in the neurotoxicity by beta-amyloid peptides and synergistic effect of inflammatory cytokines. J Exp Med 2002; 195:907–18.
21. Raaijmakers MI, Widmer DS, Maudrich M, Koch T, Langer A, Flace A, et al. A new live-cell biobank workflow efficiently recovers heterogeneous melanoma cells from native biopsies. Exp Dermatol 2015;24:377–80.
22. Carlsson J, Yuhas JM. Liquid-overlay culture of cellular spheroids. Recent Result. Cancer Res 1984;95:1–23.
23. Levesque MP, Cheng PF, Raaijmakers MI, Saltari A, Dummer R. Metastatic melanoma moves on: translational science in the era of personalized medicine. Cancer Metastasis Rev 2017;36:7–21.
24. Beaumont KA, Mohana-Kumaran N, Haass NK. Modeling melanoma *in vitro* and *in vivo*. Healthcare 2013;2:27–46.
25. Bootorabi F, Manouchehri H, Changizi R, Barker H, Palazzo E, Saltari A, et al. Zebrafish as a model organism for the development of drugs for skin cancer. Int J Mol Sci 2017;18:E1550.
26. Skeldal S, Matusica D, Nykjaer A, Coulson EJ. Proteolytic processing of the p75 neurotrophin receptor: a prerequisite for signalling?: Neuronal life, growth and death signalling are crucially regulated by intra-membrane proteolysis and trafficking of p75(NTR). Bioessays 2011;33:614–25.
27. Pathak A, Carter BD. Retrograde apoptotic signaling by the p75 neurotrophin receptor. Neuronal Signal 2017;1NS20160007.
28. Bertrand MJ, Kenchappa RS, Andrieu D, Leclercq-Smekens M, Nguyen HN, Carter BD, et al. NRAGE, a p75NTR adaptor protein, is required for developmental apoptosis in vivo. Cell Death Differ 2008;15:1921–9.
29. Selimovic D, Sprenger A, Hannig M, Haïkel Y, Hassan M. Apoptosis related protein-1 triggers melanoma cell death via interaction with the juxtamembrane region of p75 neurotrophin receptor. J Cell Mol Med 2012;16:349–61.
30. Kadowaki H, Nishitoh H, Urano F, Sadamitsu C, Matsuzawa A, Takeda K, et al. Amyloid beta induces neuronal cell death through ROS-mediated ASK1 activation. Cell Death Differ 2005;12:19–24.
31. Cheignon C, Tomas M, Bonnefont-Rousselot D, Faller P, Hureau C, Collin F. Oxidative stress and the amyloid beta peptide in Alzheimer's disease. Redox Biol 2018;14:450–64.
32. Ngo M, Han A, Lakatos A, Sahoo D, Hachey SJ, Weiskopf K, et al. Antibody therapy targeting CD47 and CD271 effectively suppresses melanoma metastasis in patient-derived xenografts. Cell Rep 2016;16:1701–16.
33. Kenchappa RS, Zampieri N, Chao MV, Barker PA, Teng HK, Hempstead BL, et al. Ligand-dependent cleavage of the P75 neurotrophin receptor is necessary for NRIF nuclear translocation and apoptosis in sympathetic neurons. Neuron 2006;50:219–32.
34. Zhong M, Wang Y, Muhammad FN, Gao J, Bian C. The p75NTR and its carboxyl-terminal fragment exert opposing effects on melanoma cell proliferation and apoptosis via modulation of the NF-κB pathway. FEBS Open Bio 2020; 11:226–36.
35. Kenchappa RS, Tep C, Korade Z, Urra S, Bronfman FC, Yoon SO. p75 neurotrophin receptor-mediated apoptosis in sympathetic neurons involves a biphasic activation of JNK and up-regulation of tumor necrosis factor-α-converting enzyme/ADAM17. J Biol Chem 201025;285:20358–68.
36. Casley CS, Canevari L, Land JM, Clark JB, Sharpe MA. Beta-amyloid inhibits integrated mitochondrial respiration and key enzyme activities. J Neurochem 2002;80:91–100.
37. Carrillo-Mora P, Luna R, Colín-Barenque L. Amyloid beta: multiple mechanisms of toxicity and only some protective effects? Oxid Med Cell Longev 2014;2014: 795375.
38. Veloria JR, Chen L, Li L, Breen GAM, Lee J, Goux WJ. Novel cell-penetrating-amyloid peptide conjugates preferentially kill cancer cells. Medchemcomm 2017; 9:121–30.
39. Maji SK, Schubert D, Rivier C, Lee S, Rivier JE, Riek R. Amyloid as a depot for the formulation of long-acting drugs. PLoS Biol 2008;6:e17.